9194 *Biochemistry* **2009,** *48,* 9194–9201
DOI: 10.1021/bi9012758

BIOCHEMISTRY
including biophysical chemistry & molecular biology
Article

Inhibition of *Neisseria meningitidis* Sialic Acid Synthase by a Tetrahedral Intermediate Analogue[†,‡]

Feng Liu,[§,⊥] Ho Jun Lee,[∥,⊥] Natalie C. J. Strynadka,[∥] and Martin E. Tanner*[,§]

[§]*Department of Chemistry, University of British Columbia, Vancouver, British Columbia, Canada V6T 1Z1, and* [∥]*Department of Biochemistry and Molecular Biology and The Centre for Blood Research, University of British Columbia, Vancouver, British Columbia, Canada V6T 1Z3* [⊥]*These authors contributed equally to the manuscript*

Received July 24, 2009; Revised Manuscript Received August 26, 2009

ABSTRACT: The *Neisseria meningitidis* sialic acid synthase (NeuB) catalyzes the metal-dependent condensation of *N*-acetylmannosamine (ManNAc) and phosphoenolpyruvate (PEP) to generate *N*-acetylneuraminic acid (NeuAc or sialic acid). *N. meningitidis* is a causative agent of meningitis and produces a capsular polysaccharide comprised of polysialic acid. This allows it to evade the immune system of the host by an act of molecular mimicry. This work describes the synthesis and characterization of the first potent inhibitor of sialic acid synthase. The inhibitor is a stable deoxy analogue of the tetrahedral intermediate presumed to form in the NeuB reaction and was synthesized as a mixture of stereoisomers at the key tetrahedral center. Inhibition studies demonstrate that one stereoisomer binds more tightly than the other and that the more potent isomer binds with micromolar affinity. An X-ray crystallographic analysis of the NeuB·inhibitor·Mn^{2+} complex solved to a resolution of 1.75 Å shows that the more tightly bound stereoisomer bears a (2*R*)-configuration. This suggests that the tetrahedral intermediate formed in the NeuB reaction also bears a (2*R*)-configuration. This analysis is consistent with a mechanism whereby the active site metal plays at least two roles during catalysis. First, it serves as an electrostatic catalyst and activates the aldehyde of ManNAc for attack by the alkene of PEP. Second, it serves as a source of nucleophilic water and delivers it to the *si* face of the oxocarbenium intermediate to generate a tetrahedral intermediate with a (2*R*)-configuration.

Sialic acid or *N*-acetylneuraminic acid (NeuAc)[1] is a nine-carbon α-keto acid that plays a wide variety of important biological roles (Figure 1) (*1*, *2*). In mammals, it is found as the terminal carbohydrate residue of many cell surface glycoconjugates. Thus, its structure defines the periphery of mammalian cells, and it is a key determinant in mediating cellular recognition processes (*3*, *4*). These include the binding between selectins and leukocytes in the inflammation response (*5*) and the binding of the influenza virus and mammalian cells during infection (*6*). While sialic acid is not commonly found in prokaryotes, certain pathogenic bacteria biosynthesize it as a virulence factor (*7*). Infections by *Neisseria meningitidis* and *Escherichia coli* K1 are among the leading causes of bacterial meningitis (*8*). These bacteria produce a capsular polysaccharide comprised of polysialic acid as a means of evading the host's immune system (*9*). Since polysialic acid is present as a posttranslational modification of neural cell adhesion molecules (NCAM's) (*10*), the capsular polysaccharide allows the bacterial cells to appear "human-like" via an act of molecular mimicry. Sialic acid is also found as a component of the lipooligosaccharide in *Campylobacter jejuni* (*11*).

In bacteria, sialic acid is synthesized in two steps from UDP-*N*-acetylglucosamine (UDP-GlcNAc) (*12*). The first step is catalyzed by a hydrolyzing UDP-GlcNAc 2-epimerase that generates *N*-acetylmannosamine (ManNAc) and UDP (*13*, *14*). Sialic acid synthase then condenses ManNAc and phosphoenolpyruvate (PEP) to generate *N*-acetylneuraminic acid (sialic acid, Figure 1) (*15*−*20*). In mammals, the biosynthesis differs in that ManNAc is first phosphorylated to give ManNAc 6-phosphate, and then the corresponding synthase generates *N*-acetylneuraminic acid 9-phosphate (*21*−*26*). Mechanistic studies on the bacterial sialic acid synthase have shown that it requires a divalent metal ion for catalysis (*15*, *16*, *20*). The enzyme is thought to catalyze the ring opening of ManNAc to expose the aldehyde functionality at C-1 (Figure 1). The C-3 carbon of PEP then attacks the aldehyde to form an oxocarbenium ion intermediate. This is facilitated by the metal ion that serves as an electrophilic catalyst and activates the carbonyl of the aldehyde toward attack. Water then adds to the oxocarbenium ion to

[†]This research was supported by the Natural Sciences and Engineering Research Council of Canada (NSERC) (to M.E.T.), the Canadian Institutes of Health Research (CIHR) (to N.C.J.S.), and the Howard Hughes Medical Institute International Scholar program (to N.C.J.S.). H.J.L. is supported by scholarships from the Kwanjeong Educational Foundation (Republic of Korea), Vancouver Korean−Canadian Scholarship Foundation, and the University of British Columbia. We acknowledge the Michael Smith Foundation for Health Research for scholarship and infrastructure support as well as the Canada Foundation for Innovation and British Columbia Knowledge Development Fund for infrastructure support (to N.C.J.S.).

[‡]X-ray coordinates have been deposited in the Protein Data Bank (accession code 2WQP).

*To whom correspondence should be addressed: phone, (604) 822-9453; fax, (604) 822-2847; e-mail, mtanner@chem.ubc.ca.

[1]Abbreviations: ACN, acetonitrile; DAH7PS, 2-keto-3-deoxy-D-*arabino*-heptulosonate-7-phosphate synthase; DMAP, *N*,*N*-dimethyl-4-aminopyridine; KDO8PS, 2-keto-3-deoxy-D-*manno*-octulosonate-8-phosphate synthase; ManNAc, *N*-acetylmannosamine; NCAM, neural cell adhesion molecule; NeuAc, *N*-acetylneuraminic acid; PEP, phosphoenolpyruvate; TIM, triose-phosphate isomerase.

 Published on Web 08/31/2009

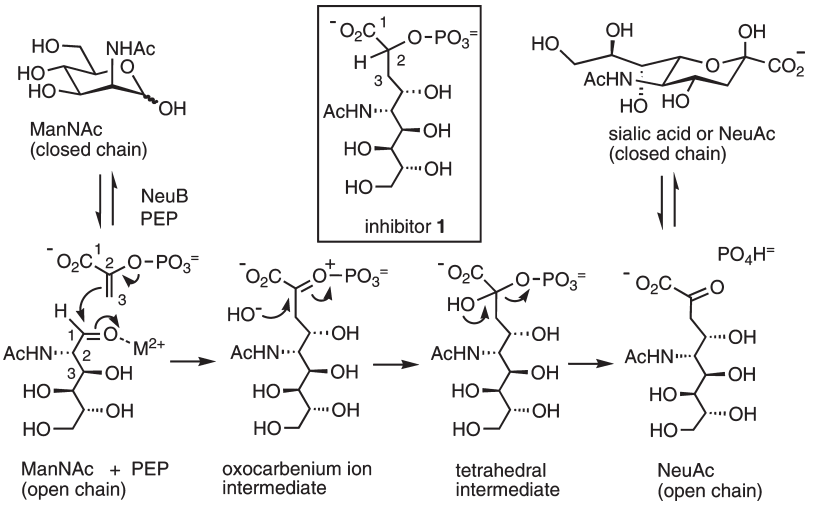

FIGURE 1: Proposed mechanism of the reaction catalyzed by sialic acid synthase (NeuB or *N*-acetylneuraminic acid synthase). The insert shows the structure of inhibitor **1**.

generate a tetrahedral intermediate. A subsequent loss of phosphate gives the open chain form of sialic acid that will readily cyclize to the pyranose form in solution.

Support for this mechanism comes from studies on the *N. meningitidis* sialic acid synthase, NeuB (*15*). When PEP bearing an ^{18}O-isotopic label in the phosphate bridging position ([2-^{18}O]-PEP) was used as a substrate, the enzymatic reaction generated ^{18}O-labeled phosphate as a product. This confirms that the loss of phosphate proceeds via a C−O bond cleavage mechanism, as is proposed to occur during the collapse of the tetrahedral intermediate. A crystallographic analysis of the synthase in a complex with *N*-acetylmannositol (substrate reduced at C-1), PEP, and Mn^{2+} also supports the mechanism (*15*). The use of the reduced substrate prevents the reaction from occurring and provides an excellent model for the Michaelis complex formed during catalysis. The C-1 hydroxyl of the substrate analogue is coordinated to Mn^{2+}, as would be expected if the normal role of the metal ion were to activate the C-1 aldehyde via electrostatic catalysis. The *si* face of the PEP is positioned directly above the *pro-S* hydrogen of *N*-acetylmannositol in the observed structure. This is consistent with a stereochemical analysis of the reaction catalyzed by the *C. jejuni* enzyme (*16*). Deuterium-labeled PEP was employed to show that the *si* face of PEP adds to the *si* face of the ManNAc aldehyde.

This work describes the synthesis and evaluation of an inhibitor that mimics the tetrahedral intermediate formed in the sialic acid synthase reaction (compound **1**, Figure 1 insert). Removal of the C-2 hydroxyl imparts stability to the compound without increasing steric bulk or altering the distribution of charges within the molecule. The compound was generated as a mixture of stereoisomers at C-2 in order to investigate the preferred orientation of groups within the active site of the enzyme. Crystallographic analysis of a complex between sialic acid synthase and the more tightly binding stereoisomer of compound **1** shows that the inhibitor bears an (*R*)-configuration at C-2. This suggests that the tetrahedral intermediate bears an (*R*)-configuration at C-2 and that a metal-bound hydroxide is delivered to the *si* face of the oxocarbenium ion intermediate during catalysis.

EXPERIMENTAL PROCEDURES

Materials and General Methods. Chemicals were purchased from Sigma-Aldrich and used without further purification unless otherwise noted. 2-Amino-6-mercapto-7-methylpurine ribonucleoside was purchased from Berry and Associates. Bacterial purine nucleoside phosphorylase was purchased from Sigma (one unit will cause the phosphorolysis of 1.0 μmol of inosine to hypoxanthine and ribose 1-phosphate per minute at pH 7.4, 25 °C). Pyridine and triethylamine were distilled over CaH_2 under an atmosphere of N_2. Protein concentrations were determined by the Bradford method using bovine serum albumin as the standard (*27*). ^{1}H and ^{31}P NMR spectra were obtained on Bruker AV400 NMR spectrometers. Mass spectra were obtained on a Waters Micromass LCT mass spectrometer using electrospray ionization (ESI-MS).

*Synthesis of Inhibitor **1**. Methyl 5-Acetamido-3,5-dideoxy-2-methylidine-4,6,7,8,9-penta-O-acetyl-D-glycero-D-galacto-2-nonulosonate* (***3***). Compound **2** was prepared in three steps from ManNAc as described previously (*28*). To a solution of compound **2** (3.72 g, 8.9 mmol) in ACN/HCl (60 mL, 20:1) were added methyl bromomethylacrylate (0.6 mL, 5 mmol) and a suspension of indium powder (100−200 mesh, 1.72 g, 15 mmol) in ACN/HCl (5 mL, 20:1). The mixture was vigorously stirred at 45 °C for 3.5 h, and then the indium clump was removed. Fresh methyl bromomethylacrylate (0.6 mL, 5 mmol) and a suspension of indium (0.5 g, 4.3 mmol) in ACN/HCl (5 mL, 20:1) were added, and the mixture was vigorously stirred at 45 °C for an additional 3 h. The reaction mixture was filtered through Celite, and the solvent was removed *in vacuo*. The resultant solid was redissolved in pyridine (40 mL), and acetic anhydride (3.62 mL, 38 mmol) and DMAP (5 mg) were added. The reaction mixture was stirred at room temperature for 16 h, and then the solvent was removed *in vacuo*. The resultant syrup was dissolved in ethyl acetate (100 mL) and washed with brine (100 mL). Silica gel column chromatography eluting with ethyl acetate (R_f = 0.3) gave a mixture of the two epimers ((4*S*):(4*R*) 3:1) as a white solid (2.01 g, 40%). Recrystallization from toluene/petroleum ether (1:1) gave the pure (4*S*)-isomer, **3**, as a white solid (1.35 g, 27%). ^{1}H NMR ($CDCl_3$, 400 MHz) δ 1.98 (s, 3H, CH_3), 2.03 (s, 3H, CH_3), 2.04 (s, 3H, CH_3), 2.04 (s, 3H, CH_3), 2.06 (s, 3H, CH_3), 2.14 (s, 3H, CH_3), 2.34 (dd, 1H, $J_{3,3}$ = 14.1 Hz, $J_{3,4}$ = 9.0 Hz, H-3), 2.59 (dd, 1H, $J_{3,3}$ = 14.0 Hz, $J_{3,4}$ = 3.9 Hz, H-3), 3.98 (dd, 1H, $J_{8,9}$ = 5.7 Hz, $J_{9,9}$ = 12.5 Hz, H-9), 4.26 (dd, 1H, $J_{8,9}$ = 3.1 Hz, $J_{9,9}$ = 12.5 Hz, H-9), 4.49 (ddd, 1H, $J_{4,5}$ = 1.5 Hz, $J_{5,6}$ = 10.3 Hz, $J_{NH,5}$ = 10.4 Hz, H-5), 5.02 (ddd, 1H, $J_{7,8}$ = 8.1 Hz, $J_{8,9}$ = 3.1 Hz, $J_{8,9}$ 5.7 = Hz, H-8), 5.14 (ddd, 1H, $J_{3,4}$ = 4.1 Hz, $J_{3,4}$ = 8.9 Hz,

$J_{4,5}$ = 1.5 Hz, H-4), 5.21 (dd, 1H, $J_{5,6}$ = 10.3 Hz, $J_{6,7}$ = 2.1 Hz, H-6), 5.35 (dd, 1H, $J_{6,7}$ = 2.1 Hz, $J_{7,8}$ = 8.1 Hz, H-7), 5.56 (d, 1H, $J_{NH,5}$ = 8.7 Hz, NH), 5.57 (d, 1H, $J_{1',1'}$ = 1.0 Hz, H-1′), 6.15 (d, 1H, $J_{1',1'}$ = 1.0 Hz, H-1′). ESI-MS (+) *m*/*z* 554 ($M + Na^+$).

Methyl 5-Acetamido-4,6,7,8,9-pentaacetoxy-2-dibenzylphosphorylnonanoate (***4***). Compound **3** (300 mg, 0.56 mmol) was dissolved in methylene chloride (30 mL), and O_3 was bubbled through the solution at −78 °C until a blue color persisted. Excess O_3 was purged by bubbling argon through the solution at −78 °C. A solution of sodium borohydride (68 mg, 1.8 mmol) in ethanol (30 mL) was then added. The mixture was allowed to stand at (a) −78 °C for 24 h or (b) 25 °C for 30 min. After removal of the solvent *in vacuo*, the solid was redissolved in ethyl acetate, which was extracted with brine and dried over anhydrous Na_2SO_4. After removal of the solvent *in vacuo*, the reduced product was used in the next step without further purification. Dibenzyl *N*,*N*-diethylphosphoramidite (600 μL, 2 mmol) was added to a solution of the reduced product (400 mg, 1.3 mmol) and 1,2,4-triazole (40 mg, 0.59 mmol) in CH_2Cl_2 (10 mL) and stirred at room temperature for 16 h. After removal of the solvent *in vacuo* the reaction mixture was redissolved in diethyl ether (50 mL). The solution was then cooled to −78 °C and stirred for 30 min after 1 mL of 30% H_2O_2 was added. The organic layer was then washed with saturated $Na_2S_2O_3$ and dried over Na_2SO_4. After removal of the solvent *in vacuo*, the resultant syrup was washed with petroleum ether and purified using silica gel column chromatography (ethyl acetate, R_f = 0.2). Compound **4** was obtained as colorless syrup and was found to be comprised of a 4.5:1 mixture of (2*S*)-**4**:(2*R*)-**4** using condition a or a 1.2:1 mixture of (2*S*)-**4**:(2*R*)-**4** using condition b. ^{1}H NMR ($CDCl_3$, 400 MHz) δ 1.92 (s, 3H, (2*S*)-CH_3), 1.93 (s, 3H, (2*R*)-CH_3), 1.98 (s, 3H, (2*S*)-CH_3), 2.00 (s, 3H, (2*R*)-CH_3), 2.019 (s, 3H, CH_3), 2.023 (s, 3H, CH_3), 2.031 (s, 3H, CH_3), 2.077 (s, 3H, (2*R*)-CH_3), 2.092 (s, 3H, (2*S*)-CH_3), 2.1 (m, 2H, H-3), 3.96 (dd, 1H, $J_{8,9a}$ = 5.7 Hz, $J_{9a,9b}$ = 12.4 Hz, (2*S*)-H-9a), 4.06 (dd, 1H, $J_{8,9a}$ = 6.6 Hz, $J_{9a,9b}$ = 6.7 Hz, (2*R*)-H-9a), 4.18 (dd, 1H, $J_{8,9b}$ = 2.5 Hz, $J_{9a,9b}$ = 6.7 Hz, (2*R*)-H-9b), 4.25 (dd, 1H, $J_{8,9b}$ = 2.8 Hz, $J_{9a,9b}$ = 12.4 Hz, (2*S*)-H-9b), 4.46 (ddd, 1H, $J_{4,5}$ = 1.5 Hz, $J_{5,6}$ = 10.4 Hz, $J_{NH,5}$ = 10.5 Hz, (2*S*)-H-5), 4.60 (ddd, 1H, $J_{4,5}$ = 1.5 Hz, $J_{5,6}$ = 10.4 Hz, $J_{NH,5}$ = 10.5 Hz, (2*R*)-H-5), 4.88 (ddd, 1H, $J_{3,4}$ = 4.6 Hz, $J_{3,4}$ = 8.2 Hz, $J_{4,5}$ = 1.5 Hz, H-4), 5.00 (ddd, 1H, $J_{7,8}$ = 8.1 Hz, $J_{8,9a}$ = 5.7 Hz, $J_{8,9b}$ = 3.0 Hz, H-8), 5.05−5.17 (m, 5H, Bn-CH_2 and H-2), 5.22 (dd, 1H, $J_{5,6}$ = 10.4 Hz, $J_{6,7}$ = 1.8 Hz, (2*S*)-H-6), 5.25 (dd, 1H, $J_{5,6}$ = 10.4 Hz, $J_{6,7}$ = 1.8 Hz, (2*R*)-H-6), 5.33 (dd, 1H, $J_{6,7}$ = 1.8 Hz, $J_{7,8}$ = 8.1 Hz, (2*S*)-H-7), 5.37 (dd, 1H, $J_{6,7}$ = 1.8 Hz, $J_{7,8}$ = 8.1 Hz, (2*R*)-H-7), 5.65 (d, 1H, $J_{NH,5}$ = 10.5 Hz, (2*R*)-NH), 5.70 (d, 1H, $J_{NH,5}$ = 10.5 Hz, (2*S*)-NH), 7.34 (m, 10H, Bn). ESI-MS (+) *m*/*z* 818 ($M + Na^+$).

5-Acetamido-4,6,7,8,9-pentahydroxy-2-phosphorylnonanoic Acid Ditriethylammonium Salt (***1***). To a solution of **4** (80 mg, 0.10 mmol) in methanol (20 mL) was added Pd/C (10%, 30 mg), and the mixture was stirred under H_2 (1 atm) for 1 h. After filtration through Celite and removal of the solvent *in vacuo*, the resulting solid was dissolved in 1:1 MeOH/H_2O (20 mL) containing 10% triethylamine (TEA) and was allowed to stand at −20 °C for 14 h. After removal of the methanol *in vacuo*, the remaining aqueous solution was diluted with distilled H_2O and lyophilized to dryness. The solid was then purified by passage through a Bio-Gel P-2 column (2.5 cm × 44 cm) eluting with distilled water (0.2 mL min^{-1}). The fractions containing inhibitor **1**, as analyzed by negative ESI-MS, were lyophilized twice with distilled water to give **1** as a white solid (25 mg, 42%). The ratio of (2*S*)-**1**:(2*R*)-**1** reflected the ratio of (2*S*)-**4**:(2*R*)-**4** used in the reaction, as determined by ^{31}P NMR spectroscopy. Due to the presence of many overlapping signals, ^{1}H and ^{13}C NMR data are only given for the major isomer (2*S*)-**1** obtained from deprotection of the 4.5:1 mixture of (2*S*)-**4**:(2*R*)-**4**. ^{1}H NMR ((2*S*)-**1**, D_2O, 400 MHz) δ 1.29 (t, 2H, TEA CH_3), 1.68 (ddd, 1H, $J_{3a,3b}$ = 11.8 Hz, $J_{3a,2}$ = 11.0 Hz, H-3a), 1.94 (dd, 1H, $J_{3a,3b}$ = 12.1 Hz, $J_{3b,4}$ = 11.0 Hz, H-3b), 2.07 (s, 3H, CH_3), 3.21 (q, 2H, TEA CH_2) 3.48 (dd, 1H, $J_{7,8}$ = 8.9 Hz, H-7), 3.65 (dd, 1H, $J_{8,9a}$ = 6.4 Hz, $J_{9a,9b}$ = 11.8 Hz, H-9a), 3.79 (ddd, 1H, $J_{7,8}$ = 8.9 Hz, $J_{8,9a}$ = 6.3 Hz, $J_{8,9b}$ = 2.7 Hz, H-8), 3.85 (dd, 1H, $J_{8,9b}$ = 2.6 Hz, $J_{9a,9b}$ = 11.8 Hz, H-9b), 3.94 (dd, 1H, $J_{5,6}$ = 10.1 Hz, H-5), 4.01 (dd, 1H, $J_{5,6}$ = 10.0 Hz, H-6), 4.37 (dd, 1H, $J_{3,4}$ = 11 Hz, H-4), 4.54 (ddd, 1H, $J_{2,3}$ = 2.8 Hz, $J_{2,3}$ = 10 Hz, $J_{2,P}$ = 10 Hz, H-2). ^{13}C NMR ((2*S*)-**1**, MeOD, 100 MHz) δ 9.3 (TEA), 22.6 (CH_3), 40.3 (C-3), 47.5 (TEA), 56.4 (C-5), 65.4 (C-9), 65.9 (C-4), 69.9 (C-6), 71.8 (C-7), 72.5 (C-8), 74.8 (C-2), 174.6 (C=O), 180.2 (O=C−OH). ^{31}P NMR (D_2O, pD 7, 162 MHz) δ 2.30 ((2*R*)-**1**), 2.75((2*S*)-**1**). HRMS calculated for $C_{11}H_{21}NO_{12}P$ ($M - H^+$) 390.0801, found 390.0806.

Measurement of Inhibition Kinetics. Inhibition kinetics were measured using a slight modification of a previously reported continuous coupled assay for phosphate (*29*, *30*). His-tagged NeuB was generated and purified as described previously (*15*). A cuvette containing Tris-HCl buffer (pH 7.0, 100 mM), $MnCl_2$ (1 mM), PEP (variable, 50 μM to 1 mM), His-tagged NeuB (5 μg), purine nucleoside phosphorylase (bacterial, Sigma, 5 units, previously buffer exchanged to 20 mM Tris-HCl, pH 7.0), 2-amino-6-mercapto-7-methylpurine ribonucleoside (200 μM), and inhibitor **1** (variable, 0−20 μM of the 4.5:1 mixture of (2*S*)-**1**:(2*R*)-**1**) was preincubated for 20 min at 37 °C. The enzymatic reaction was initiated by addition of ManNAc (10 mM). Rates were measured by monitoring the increase of absorption at 360 nm (ε = 11000 M^{-1} cm^{-1}). Kinetic parameters were determined by fitting initial velocities to the Michaelis−Menten equation using GraFit 5.0 (Erithacus software).

Cloning, Overexpression, and Purification of NeuB for Crystallization. All molecular biology procedures were performed as described previously (*15*). Briefly, the untagged NeuB enzyme was cloned into the pCWori+ vector and subsequently transformed into the electrocompetent *E. coli* cell (BL21 λDE3; Novagen) for expression. Overexpression of NeuB was carried out by induction with 0.5 mM isopropyl β-D-galactopyranoside (IPTG) at OD_{600} ∼ 0.6 with overnight shaking at 20 °C. Cells were harvested by centrifuging at 5000 rpm (6200*g*) for 15 min, resuspended, and lysed at 20000 psi using a high-pressure homogenizer (Avestin) in the presence of EDTA-free protease inhibitor cocktail (Roche Applied Science). The lysate was subsequently centrifuged at 40000 rpm (161000*g*) for 35 min, and the supernatant containing the target protein was purified by a series of chromatographic procedures including ion-exchange and gel filtration steps. Purified NeuB enzyme was concentrated to 10 mg/mL and used for crystallization.

Crystallization, Data Collection, and Structure Refinement. Purified NeuB enzyme was crystallized at 18 °C in the presence of 10 mM $MnCl_2$ and 1.50−1.55 M malic acid (pH 6.2) using the hanging-drop vapor diffusion technique and subsequently soaked in 2 M sodium phosphate (pH 6.2) for 24 h with 10 mM $MnCl_2$ and 3 mM of the 4.5:1 mixture of (2*S*)-**1**:(2*R*)-**1**. The soaked crystal was transferred into the mother liquor containing 25% ethylene glycol for 10 s and frozen in liquid nitrogen prior to data collection. X-ray diffraction data were

Table 1: Data Collection and Refinement Statistics

	NeuB + inhibitor **1**
Data Collection	
X-ray source	ALS 4.2.2
wavelength (Å)	0.9790
resolution (Å)[a]	40−1.75 (1.84−1.75)
space group	$P2_12_12$
a (Å)	58.62
b (Å)	75.74
c (Å)	77.36
α, β, γ (deg)	90, 90, 90
R_{sym} (%)[a]	10.5 (46.1)
$I/\sigma(I)$[a]	12.4 (2.2)
completeness (%)[a]	99.3 (97.0)
unique reflections[a]	35158 (4926)
redundancy[a]	4.0 (3.6)
Refinement Statistics	
average B-factors (Å^2)	
protein	9.0
ligand	13.8
water	18.4
Ramachandran statistics	
favored regions (%)	98.9
allowed regions (%)	1.1
R_{work} (%)	16.3
R_{free} (%)	19.7
rms[b] bonds (Å)	0.011
rms angles (deg)	1.202

[a]Values in parentheses represent the highest resolution shell. [b]rms, root mean square.

collected at 100 K under a nitrogen stream at the beamline 4.2.2 of the Advanced Light Source (Berkeley, CA) coupled to a NOIR-1 CCD detector. Collected data were processed by MOSFLM (*31*) and SCALA (*32*). The inhibitor **1** bound NeuB crystal belongs to the space group $P2_12_12$ with unit cell dimensions a = 58.62, b = 75.74, and c = 77.36 Å and contains one molecule in the asymmetric unit. Scaled data were directly used for the structure refinement by REFMAC5 (*33*) with the coordinate of NeuB as a starting model (PDB accession code 1XUZ). The required parameter file for inhibitor **1** was generated from the Dundee PRODRG2 server (*34*), and all structural figures were produced using PyMOL (*35*). Statistics for data collection and refinement are summarized in Table 1.

RESULTS AND DISCUSSION

*Synthesis of Inhibitor **1***. The overall strategy used in the synthesis of inhibitor **1** involved the addition of a three-carbon masked pyruvate unit to the peracetylated open chain form of ManNAc, **2** (Figure 2). The aldehyde of ManNAc was first protected using hydroxylamine, and the exposed hydroxyl groups were peracetylated using acetic anhydride. Ozonolysis was used to unmask the aldehyde functionality and gave compound **2** in three steps, as reported previously (*28*). An indium-mediated addition of methyl bromomethylacrylate, followed by acetylation with acetic anhydride, generated compound **3** as a 3:1 ratio of isomers at C-4. Column chromatography, followed by recrystallization, gave the major isomer of **3** bearing the required (*S*)-configuration at C-4. Previous studies on indium-mediated couplings of closely related compounds also show this selectivity and demonstrate that the major isomer bears a *syn* relationship

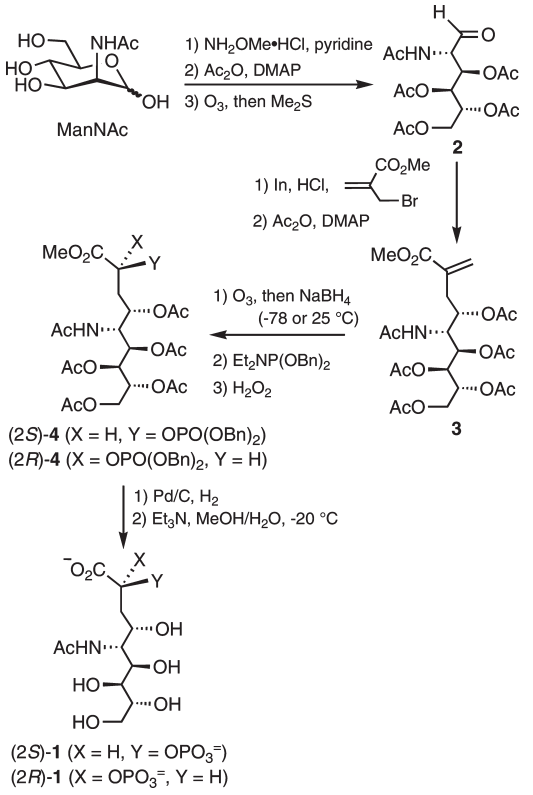

FIGURE 2: The synthetic route used in the preparation of inhibitor **1**.

between the newly formed hydroxyl group and the acetamido group, consistent with a chelate-controlled delivery (*36*−*38*). Ultimately, crystallographic analysis of the complex between the final inhibitor **1** and sialic acid synthase confirmed this stereochemical outcome (vide infra). Treatment of compound **3** with ozone exposed the ketone functionality at C-2, and reduction with sodium borohydride followed by phosphorylation gave compound **4** as a mixture of stereoisomers. When the reduction was carried out at −78 °C, a 4.5:1 mixture of (2*S*)-**4**:(2*R*)-**4** was obtained, and when the reduction was carried out at 25 °C, a 1.2:1 mixture of (2*S*)-**4**:(2*R*)-**4** was obtained. These isomers were not separable by conventional silica gel chromatography and were therefore carried on as a mixture. Deprotection of compound **4** was achieved via hydrogenolysis of the benzyl phosphate groups, followed by mild ester hydrolysis using triethylamine in MeOH/H_2O at −20 °C. Size exclusion chromatography gave pure inhibitor **1** as either a 4.5:1 mixture of (2*S*)-**1**:(2*R*)-**1** or a 1.2:1 mixture of (2*S*)-**1**:(2*R*)-**1**, depending on the reduction conditions used to prepare compound **4**. The assignment of configuration at C-2 in compounds **4** and **1** was made by first determining which of the two isomers of **1** is a better inhibitor and then by analyzing the structure of the inhibited enzyme (vide infra).

*Kinetic Evaluation of Inhibitor **1***. Kinetic constants for the inhibition of the *N. menigitidis* sialic acid synthase by compound **1** were obtained using a continuous coupled assay for phosphate release (*29*, *30*). Initial studies were performed on the 4.5:1 mixture of (2*S*)-**1**:(2*R*)-**1** and indicated that compound **1** acted as a strong and slow binding inhibitor. Therefore, prior to each kinetic analysis, the enzyme was preincubated in the presence of the inhibitor (variable amounts), PEP (variable amounts), and Mn^{2+} (1 mM) for 20 min to ensure that binding equilibration had occurred. The reactions were then initiated by the addition of a saturating amount of ManNAc (10 mM). Compound **1** was found to act as a competitive inhibitor against PEP with an

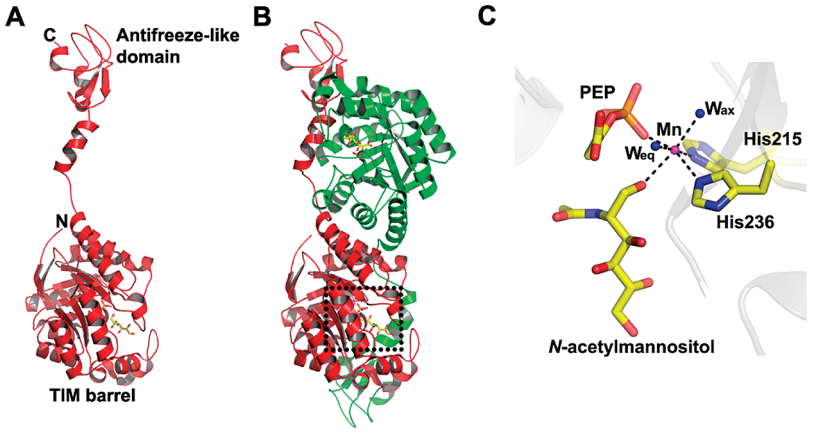

FIGURE 3: Overall structure and substrate binding site of NeuB (ref *15*, PDB accession code 1XUZ). (A) Ribbon representation of the NeuB monomer structure showing the TIM barrel and antifreeze-like domains. (B) Domain-swapped homodimeric structure of NeuB with each monomer colored red or green. Bound substrates which delineate the active site (*N*-acetylmannositol, PEP) are shown in CPK colored stick representations. The active site is formed at the interface of two monomers as highlighted by the black dotted box. (C) Active site of NeuB focusing on the essential metal coordination. The metal ion is shown as a magenta sphere (relative radius reduced for clarity), and histidine residues (His215, His236) and bound substrates are shown as a CPK colored stick model (carbons in yellow, oxygens in red, nitrogens in blue, phosphates in orange). Water molecules (W_{ax}, W_{eq}) are shown as blue spheres. Hydrogen bonds are represented by black dotted lines.

apparent K_i value of 3.1 ± 0.1 μM (see Supporting Information). Identical kinetic runs using the 1.2:1 mixture of (2*S*)-**1**:(2*R*)-**1** (containing 45% (2*R*)-**1** instead of 18%) required an approximately 2.5-fold lower total inhibitor concentration in order to bring about a comparable reduction of rate. This indicates that the minor (2*R*)-isomer is responsible for at least 80% of the inhibition. The fact that the value of K_i for compound **1** is significantly lower than the value of K_M for PEP (157 μM under identical conditions) supports the notion that the inhibitor serves as a mimic of the tetrahedral intermediate presumed to form in the synthase reaction. Furthermore, the fact that one isomer binds more tightly than the other suggested that it would be possible to characterize a complex containing only this isomer.

*Crystallographic Analysis of the Complex between Inhibitor **1** and Sialic Acid Synthase*. Previous crystallographic studies showed that the *N. meningitidis* sialic acid synthase, NeuB, exists as a domain-swapped homodimer with 2-fold symmetry coincident with that of the 2-fold symmetry axis of the orthorhombic crystal form (Figure 3A,B) (*15*). Each monomer consists of an N-terminal $(\alpha/\beta)_8$ barrel (TIM barrel) and a "pretzel-shaped" C-terminal domain that bears high sequence identity and structural similarity to the ice binding type III antifreeze protein. The C-terminal domain of one subunit caps the TIM barrel of the opposing subunit and is intimately involved in hydrogen-bonding interactions in the active site. This earlier structure of NeuB was solved to 2.2 Å resolution as a complex with *N*-acetylmannositol (substrate reduced at C-1), PEP, and Mn^{2+}, providing an excellent model of the Michaelis complex (Figure 3C). The metal ion was coordinated in an octahedral manner with His-215, His-236, the phosphate of PEP, and a bound water (W_{eq}) serving as the equatorial ligands and with the C-1 hydroxyl of *N*-acetylmannositol and a second bound water (W_{ax}) serving as the axial ligands. The observation of direct coordination between the hydroxyl of *N*-acetylmannositol and the metal ion was consistent with the proposed role of the metal in activating the aldehyde of ManNAc in the normal reaction mechanism. This structure also showed that the *si* face of PEP faces the C-1 of the *N*-acetylmannositol, consistent with the reported stereochemical outcome of the synthase reaction (*16*). The carboxylate of PEP was twisted by 30° with respect to the

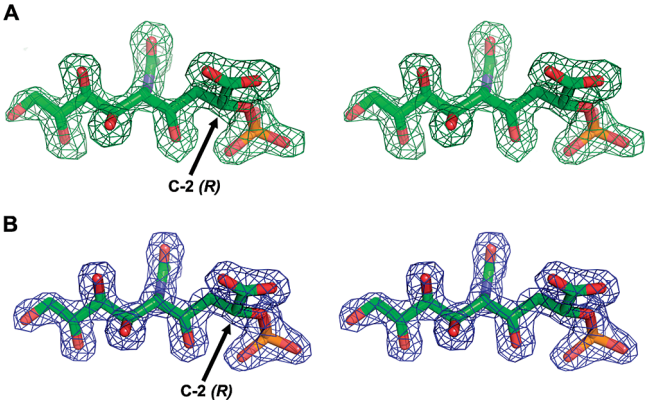

FIGURE 4: Observed electron density of inhibitor (2*R*)-**1**. Stereoview of the observed electron density of the NeuB-bound inhibitor **1** in (A) the initial $F_o - F_c$ map contoured at 3.5σ and (B) the refined $2F_o - F_c$ map contoured at 1.5σ. The (*R*) configuration of inhibitor **1** is highlighted with an arrow at the C-2 position. Carbon atoms are represented in green. Non-carbon atoms are colored according to atom type (N, blue; O, red; P, orange).

alkene functionality, presumably to reduce conjugation and increase the nucleophilicity of the alkene.

In order to obtain a complex with inhibitor **1**, NeuB was first crystallized in the presence of 10 mM $MnCl_2$ and 1.50−1.55 M malic acid (pH 6.2) to generate the malic acid/Mn^{2+} complex described previously (*15*). The NeuB crystals were then soaked in 2 M phosphate buffer (pH 6.2) containing 10 mM $MnCl_2$ and 3 mM of the 4.5:1 mixture of (2*S*)-**1**:(2*R*)-**1**. This resulted in the formation of a NeuB·inhibitor **1**·Mn^{2+} complex that could be structurally characterized to a resolution of 1.75 Å with excellent stereochemical quality and R_{work}/R_{free} values (0.163/0.197) (Table 1). The bound inhibitor **1** was clearly visible at 3.5σ in the $F_o - F_c$ maps (before any additional refinement) and was judged to be fully occupied within the active site in refined $2F_o - F_c$ maps (Figure 4). Inspection of the structure clearly shows that only a single stereoisomer, (2*R*)-**1**, is present, indicating that the enzyme had selected this less prevalent but tighter binding isomer from the incubation mixture. The overall structure was very similar to that of NeuB·*N*-acetylmannositol·PEP·Mn^{2+}, with a

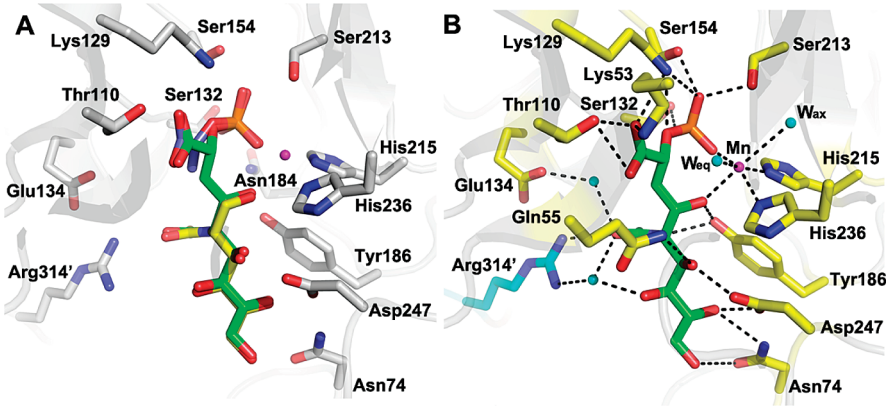

FIGURE 5: The active site of NeuB complexed with inhibitor (2*R*)-**1**. (A) Comparison of active sites between the NeuB·inhibitor **1**·Mn^{2+} and the NeuB·*N*-acetylmannositol·PEP·Mn^{2+} structures. Interacting amino acid residues are shown in CPK coloring with carbons in gray. Carbon atoms in the inhibitor **1**, *N*-acetylmannositol, and PEP are displayed with green, yellow, and light blue, respectively. Lys53 and Gln55 have been omitted for clarity. (B) Active site of the NeuB·inhibitor **1**·Mn^{2+} complex. All interacting amino acid residues are shown in CPK with carbons in yellow from one monomer and in cyan from the adjacent monomer with black dotted lines representing hydrogen bonds. Carbon atoms in inhibitor **1** are displayed with green, and non-carbon atoms are colored according to atom type (N, blue; O, red; P, orange). Manganese ion and water molecules are represented as magenta and cyan spheres, respectively. Asn184 has been omitted for clarity.

root-mean-square deviation (rmsd) of 0.16 Å on all 345 Cα atoms. The phosphate and carboxylate groups of **1** occupy similar positions and engage in analogous hydrogen-bonding interactions to the corresponding groups of PEP and *N*-acetylmannositol in the previous structure (Figure 5A). The phosphate group of **1** establishes a number of hydrogen bonds to various conserved residues including Ser-132, Ser-154, Ser-213, and Lys-129, as well as Asn-184 in the active site (Figure 5B). The carboxylate of **1** interacts electrostatically with the conserved lysine residues (Lys-53, Lys-129) as well as via a hydrogen bond with Thr-110. All hydroxyl groups of inhibitor **1** are also involved in the extensive hydrogen-bonding network through a series of conserved residues (Gln-55, Tyr-186, and Asp-247) and water molecules. The *N*-acetylamino group of inhibitor **1** also interacts with the enzyme via water-mediated contacts. One water molecule bridges between the carbonyl moiety of the *N*-acetylamino group and the side chain carboxylate of Glu-134. The other water molecule interacts with both the carbonyl moiety of the *N*-acetylamino group and the C-7 hydroxyl group of inhibitor **1** and also establishes a direct contact to the conserved Arg-314′ residue from the neighboring monomer in the homodimeric complex.

An analysis of the tetrahedral geometry at C-2 clearly indicates an (*R*)-configuration of the bound inhibitor and provides the basis for the assignment of stereochemistry of the tighter binding isomer. Assuming that this stereochemical preference reflects a resemblance to the tetrahedral intermediate, then the intermediate is also expected to bear an (*R*)-configuration at C-2. This would indicate that the reaction mechanism involves an attack of water onto the *si* face of the oxocarbenium ion intermediate (Figure 6). The (2*R*)-configuration orients the C-2 hydrogen of inhibitor **1** toward the Mn^{2+} ion and suggests that in the actual tetrahedral intermediate the C-2 hydroxyl may serve as a ligand for the metal. It also implies that the metal may play a dual role in catalysis, both as an electrostatic catalyst that activates the aldehyde of ManNAc and as a source of the activated water molecule that attacks the oxocarbenium ion intermediate (Figure 6). In the NeuB·*N*-acetylmannositol·PEP·Mn^{2+} structure, the equatorial metal-bound water molecule (W_{eq}) is positioned 2.8 Å away from the *si* face of the bound PEP (3.1 Å away from C-2 of PEP) and is a likely candidate to play the role of the

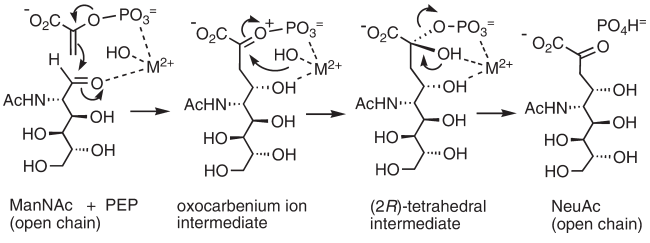

FIGURE 6: Revised mechanism of the reaction catalyzed by sialic acid synthase outlining the proposed stereochemistry of the tetrahedral intermediate and the dual role played by the Mn^{2+} ion.

nucleophile (Figure 3). Glu-25 and Glu-234 are hydrogen-bonded to W_{eq} and serve as reasonable candidates for the basic residue that deprotonates W_{eq} during its addition to the oxocarbenium ion intermediate. In the structure of NeuB·inhibitor **1**·Mn^{2+}, the electron density corresponding to the Mn^{2+} ion indicates only partial occupancy (50%) based on resulting maps and temperature factors. The partial occupancy of the metal cofactor indicates that the manganese ion binds weakly to the NeuB·inhibitor **1** complex. This notion is further supported by the determination of NeuB·inhibitor **1** structures devoid of bound metal cofactor that were obtained during various soaking trials. The manganese ion of the NeuB·inhibitor **1**·Mn^{2+} complex was coordinated in the active site with a significantly distorted octahedral arrangement, whereas the previously reported NeuB·*N*-acetylmannositol·PEP·Mn^{2+} complex displayed the much more regular octahedral geometry typical of Mn^{2+} binding coordination spheres. The metal−ligand interactions are largely maintained in the NeuB·inhibitor **1**·Mn^{2+} structure, except that W_{eq} has moved 0.6 Å away from the bound inhibitor and the distance between the metal and W_{ax} has increased by 0.8 Å (Figure 5B). In addition, W_{ax} loses the contact with the carboxylate of Glu-234 and now interacts with Ser-213 and main chain carbonyls of Asp-214 and Glu-234, thereby moving ~25° from its position in the previous structure to create the distorted octahedral geometry. The partial occupancy and distorted geometry of the bound metal suggest that the binding of inhibitor **1** disturbs the coordination sphere and likely impairs binding somewhat. One explanation may lie in the fact that the C-2 hydrogen of the inhibitor is oriented toward the metal and

thereby has displaced W_{eq} from its preferred position. In the normal reaction mechanism, the C-2 hydroxyl group of the tetrahedral intermediate would occupy this coordination site and no steric clash would result. An alternative explanation for the perturbed metal binding/geometry could be that a conformational change normally accompanies the formation of the tetrahedral intermediate but that soaking with the inhibitor is not sufficient to induce the same change in the solid state. In this event, the active site would not be in an optimal conformation to bind both inhibitor **1** and the metal ion, and the metal binding could be impaired. Unfortunately, our attempts to obtain a structure by cocrystallization were unsuccessful.

CONCLUSIONS

The bacterial sialic acid synthases are most closely related to the mammalian sialic acid synthases and to other metal-dependent bacterial enzymes that catalyze the biosynthesis of structurally similar α-keto acids. These include pseudaminic acid synthase (NeuB shares 35% identity with *C. jejuni* enzyme) and *N*,*N*-diacetyllegionaminic acid synthase (NeuB shares 61% identity with the *Legionella pneumophila* enzyme) (*29*, *39*, *40*). Sialic acid synthase is more distantly related to other α-keto acid synthases such as 2-keto-3-deoxy-D-*manno*-octulosonate-8-phosphate synthase (KDO8PS) and 2-keto-3-deoxy-D-*arabino*-heptulosonate-7-phosphate synthase (DAH7PS) (*41*−*43*). The latter enzymes do not share significant sequence identity with NeuB (< 10%) and do not possess the unique C-terminal domain, yet are known to adopt a TIM barrel protein fold (*44*, *45*). While all of the α-keto acid synthases utilize a C−O bond cleavage mechanism (*15*, *29*, *40*, *46*, *47*), the requirement for a metal ion cofactor is not universal (*48*−*50*).

Previous studies on the generation of mechanism-based inhibitors of the α-keto acid synthases have focused on the KDO8PS and DAH7PS enzymes (*51*−*54*). Much of that work centered on the preparation of amine-bearing derivatives that mimic the oxocarbenium ion intermediate thought to form during catalysis. One report described the synthesis of phosphonate-based analogues of the tetrahedral intermediates formed by these enzymes; however, kinetic studies were not presented (*55*). This report describes the first reported inhibitor of a sialic acid synthase, inhibitor **1**, which is a 2-deoxy analogue of the putative tetrahedral intermediate. The compound was synthesized as a mixture of stereoisomers at C-2 in order to probe the preference of the active site in binding a given configuration. Inhibition studies and structural analysis confirm that the inhibitor bearing the (2*R*)-configuration is bound more tightly than the other. This suggests that the tetrahedral intermediate also bears a (2*R*)-configuration and that the C-2 hydroxyl group is directed toward the active site metal ion. The mechanistic implications of this arrangement are that the metal serves not only to activate the carbonyl of ManNAc for attack by PEP in the first step of the reaction but also to deliver hydroxide to the oxocarbenium ion intermediate in the second step of the reaction (Figure 6). While stereochemical analyses based on the use of intermediate analogues often provide key insights into the mechanisms of enzymatic reactions, it must be mentioned that they can be misleading. An example of this can be found with the enzyme 5-enolpyruvylshikimate-3-phosphate synthase where a phosphonate-based inhibitor bearing the non-natural configuration at the transient tetrahedral center bound more tightly than the one with the natural configuration (*56*). While it is not possible to isolate the tetrahedral intermediate formed in the sialic acid synthase reaction and determine its stereochemistry directly, the preparation and analysis of additional analogues could reinforce the findings of this study. Toward that end, the syntheses of phosphonate-based analogues that retain the C-2 hydroxyl group are currently being pursued in these laboratories.

ACKNOWLEDGMENT

We thank the X-ray Crystallography Hub at the Centre for Blood Research (University of British Columbia) and the Advanced Light Source beamline 4.2.2 (Berkeley, CA) for data collection.

SUPPORTING INFORMATION AVAILABLE

Kinetic data for the inhibition of NeuB by inhibitor **1**. This material is available free of charge via the Internet at http://pubs.acs.org.

REFERENCES

1. Schauer, R. (2004) Sialic acids: fascinating sugars in higher animals and man. *Zoology 107*, 49–64.
2. Angata, T., and Varki, A. (2002) Chemical diversity in the sialic acids and related α-keto acids: an evolutionary perspective. *Chem. Rev. 102*, 439–469.
3. Traving, C., and Schauer, R. (1998) Structure, function and metabolism of sialic acids. *Cell. Mol. Life Sci. 54*, 1330–1349.
4. Varki, A. (1997) Sialic acids as ligands in recognition phenomena. *FASEB J. 11*, 248–255.
5. Varki, A. (2007) Glycan-based interactions involving vertebrate sialic-acid-recognizing proteins. *Nature 446*, 1023–1029.
6. Olofsson, S., and Bergstrom, T. (2005) Glycoconjugate glycans as viral receptors. *Ann. Med. 37*, 154–172.
7. Severi, E., Hood, D. W., and Thomas, G. H. (2007) Sialic acid utilization by bacterial pathogens. *Microbiology 153*, 2817–2822.
8. Saez-Llorens, X., and McCracken, G. H. (2003) Bacterial meningitis in children. *Lancet 361*, 2139–2148.
9. Finne, J. (1985) Polysialic acid—a glycoprotein carbohydrate involved in neural adhesion and bacterial-meningitis. *Trends Biochem. Sci. 10*, 129–132.
10. Kleene, R., and Schachner, M. (2004) Glycans and neural cell interactions. *Nat. Rev. Neurosci. 5*, 195–208.
11. Preston, A., Mandrell, R. E., Gibson, B. W., and Apicella, M. A. (1996) The lipooligosaccharides of pathogenic Gram-negative bacteria. *Crit. Rev. Microbiol. 22*, 139–180.
12. Tanner, M. E. (2005) The enzymes of sialic acid biosynthesis. *Bioorg. Chem. 33*, 216–228.
13. Murkin, A. S., Chou, W. K., Wakarchuk, W. W., and Tanner, M. E. (2004) Identification and mechanism of a bacterial hydrolyzing UDP-*N*-acetylglucosamine 2-epimerase. *Biochemistry 43*, 14290–14298.
14. Vann, W. F., Daines, D. A., Murkin, A. S., Tanner, M. E., Chaffin, D. O., Rubens, C. E., Vionnet, J., and Silver, R. P. (2004) The NeuC protein of *Escherichia coli* K1 is a UDP-*N*-acetylglucosamine 2-epimerase. *J. Bacteriol. 186*, 706–712.
15. Gunawan, J., Simard, D., Gilbert, M., Lovering, A. L., Wakarchuk, W. W., Tanner, M. E., and Strynadka, N. C. (2005) Structural and mechanistic analysis of sialic acid synthase NeuB from *Neisseria meningitidis* in complex with Mn^{2+}, phosphoenolpyruvate, and *N*-acetylmannosaminitol. *J. Biol. Chem. 280*, 3555–3563.
16. Sundaram, A. K., Pitts, L., Muhammad, K., Wu, J., Betenbaugh, M., Woodard, R. W., and Vann, W. F. (2004) Characterization of *N*-acetylneuraminic acid synthase isoenzyme 1 from *Campylobacter jejuni*. *Biochem. J. 383*, 83–89.
17. Suryanti, V., Nelson, A., and Berry, A. (2003) Cloning, over-expression, purification, and characterization of *N*-acetylneuraminate synthase from *Streptococcus agalactiae*. *Protein Expression Purif. 27*, 346–356.
18. Hwang, T.-S., Hung, C.-H., Teo, C.-F., Chen, G.-T., Chang, L.-S., Chen, S.-F., Chen, Y.-J., and Lin, C.-H. (2002) Structural characterization of *Escherichia coli* sialic acid synthase. *Biochem. Biophys. Res. Commun. 295*, 167–173.
19. Vann, W. F., Tavarez, J. J., Crowley, J., Vimr, E., and Silver, R. P. (1997) Purification and characterization of the *Escherichia coli* K1

neuB gene product *N*-acetylneuraminic acid synthetase. *Glycobiology 7*, 697–701.
20. Blacklow, R. S., and Warren, L. (1962) Biosynthesis of sialic acids by *Neisseria meningitidis*. *J. Biol. Chem. 237*, 3520–3526.
21. Chou, W. K., Hinderlich, S., Reutter, W., and Tanner, M. E. (2003) Sialic acid biosynthesis: stereochemistry and mechanism of the reaction catalyzed by the mammalian UDP-*N*-acetylglucosamine 2-epimerase. *J. Am. Chem. Soc. 125*, 2455–2461.
22. Hinderlich, S., Stäsche, R., Zeitler, R., and Reutter, W. (1997) A bifunctional enzyme catalyzes the first two steps in *N*-acetylneuraminic acid biosynthesis of rat liver. *J. Biol. Chem. 272*, 24313–24318.
23. Stasche, R., Hinderlich, S., Weise, C., Effertz, K., Lucka, L., Moorman, P., and Reutter, W. (1997) A bifunctional enzyme catalyzes the first two steps in *N*-acetylneuraminic acid biosynthesis of rat liver. *J. Biol. Chem. 272*, 24319–24324.
24. Hao, J., Vann, W. F., Hinderlich, S., and Sundaramoorthy, M. (2006) Elimination of 2-keto-3-deoxy-D-*glycero*-D-*galacto*-nonulosonic acid 9-phosphate synthase activity from human *N*-acteylneuraminic acid 9-phosphate synthase by a single mutation. *Biochem. J. 397*, 195–201.
25. Chen, H., Blume, A., Zimmerman-Kordmann, M., Reutter, W., and Hinderlich, S. (2002) Purification and characterization of *N*-acetylneuraminic acid-9-phosphate synthase from rat liver. *Glycobiology 12*, 65–71.
26. Lawrence, S. M., Huddleston, K. A., Pitts, L. R., Nguyen, N., Lee, Y. C., Vann, W. F., Coleman, T. A., and Betenbaugh, M. J. (2000) Cloning and expression of the human *N*-acetylneuraminic acid phosphate synthase gene with 2-keto-3-deoxy-D-*glycero*-D-*galacto*-nononic acid biosynthetic ability. *J. Biol. Chem. 275*, 17869–17877.
27. Bradford, M. M. (1976) A rapid and sensitive method for the quantitation of microgram quantities of protein utilizing the principle of protein-dye binding. *Anal. Biochem. 72*, 248–254.
28. Weitz, D. J., and Bednarski, M. D. (1989) Synthesis of acyclic sugar aldehydes by ozonolysis of oximes. *J. Org. Chem. 54*, 4957–4959.
29. Chou, W. K., Dick, S., Wakarchuk, W. W., and Tanner, M. E. (2005) Identification and characterization of NeuB3 from *Campylobacter jejuni* as a pseudaminic acid synthase. *J. Biol. Chem. 280*, 35922–35928.
30. Webb, M. R. (1992) A continuous spectrophotometric assay for inorganic phosphate and for measuring phosphate release kinetics in biological systems. *Proc. Natl. Acad. Sci. U.S.A. 89*, 4884–4887.
31. Leslie, A. (1992) Recent changes to the MOSFLM package for processing film and image plate data. *Joint CCP4+ESF-EAMCB Newsletter on Protein Crystallography 26*, 1.
32. Potterton, E., Briggs, P., Turkenburg, M., and Dodson, E. (2003) A graphical user interface to the CCP4 program suite. *Acta Crystallogr., Sect. D: Biol. Crystallogr. 59*, 1131–1137.
33. Murshudov, G. N., Vagin, A. A., and Dodson, E. J. (1997) Refinement of macromolecular structures by the maximum-likelihood method. *Acta Crystallogr., Sect. D: Biol. Crystallogr. 53*, 240–255.
34. Schuttelkopf, A. W., and van Aalten, D. M. (2004) PRODRG: a tool for high-throughput crystallography of protein-ligand complexes. *Acta Crystallogr., Sect. D: Biol. Crystallogr. 60*, 1355–1363.
35. DeLano, W. L. (2002) The PyMOL molecular graphics system, DeLano Scientific, San Carlos, CA.
36. Vorwerk, S., and Vasella, A. (1998) Carbocyclic analogues of *N*-acetyl-2,3-didehydro-2-deoxy-D-neuraminic acid (Neu5Ac2en, DANA): synthesis and inhibition of viral and bacterial neuraminidases. *Angew. Chem., Int. Ed. 37*, 1732–1734.
37. Paquette, L. A., Mitzel, T. M., Isaac, M. B., Crasto, C. F., and Schomer, W. W. (1997) Diastereoselection during 1,2-addition of the allylindium reagent to α-thia and α-amino aldehydes in aqueous and organic solvents. *J. Org. Chem. 62*, 4293–4301.
38. Chan, T.-H., and Lee, M.-C. (1995) Indium-mediated coupling of α-(bromomethyl)acrylic acid with carbonyl compounds in aqueous media. Concise syntheses of (+)-3-deoxy-D-*glycero*-D-*galacto*-nonulosonic acid and *N*-acetylneuraminic acid. *J. Org. Chem. 60*, 4288–4232.
39. Schoenhofen, I. C., Vinogradov, E., Whitfield, D. M., Brisson, J.-R., and Logan, S. M. (2009) The CMP-legionaminic acid pathway in *Campylobacter*: biosynthesis involving novel GDP-linked precursors. *Glycobiology 19*, 715–725.
40. Glaze, P. A., Watson, D. C., Young, N. M., and Tanner, M. E. (2008) Biosynthesis of CMP-*N*,*N*′-diacetyllegionaminic acid from UDP-*N*,*N*′-diacetylbacillosamine in *Legionella pneumophila*. *Biochemistry 47*, 3272–3282.
41. Furdui, C., Zhou, L., Woodard, R. W., and Anderson, K. S. (2004) Insights into the mechanism of 3-deoxy-D-*arabino*-heptulosonate-7-phosphate synthase (DAHP synthase) (Phe) from *E. coli* using a transient kinetic analysis. *J. Biol. Chem. 279*, 45618–45625.
42. Howe, D. L., Sundaram, A. K., Wu, J., Gatti, D. L., and Woodard, R. W. (2003) Mechanistic insight into 3-deoxy-D-*manno*-octulosonate-8-phosphate synthase and 3-deoxy-D-*arabino*-heptulosonate-7-phosphate synthase utilizing phosphorylated monosaccharide analogs. *Biochemistry 42*, 4843–4854.
43. Liang, P.-H., Lewis, J., Anderson, K. S., Kohen, A., D'Souza, F. W., Benensen, Y., and Baasov, T. (1998) Catalytic mechanism of KDO8P synthase: transient kinetic studies and evaluation of a putative reaction intermediate. *Biochemistry 37*, 16390–16399.
44. Radaev, S., Dastidar, P., Patel, M., Woodard, R. W., and Gatti, D. L. (2000) Structure and mechanism of 3-deoxy-D-*manno*-octulosonate 8-phosphate synthase. *J. Biol. Chem. 275*, 9476–9484.
45. Shumilin, I. A., Kretsinger, R. H., and Bauerle, R. H. (1999) Crystal structure of phenylalanine-regulated 3-deoxy-D-*arabino*-heptulosonate 7-phosphate synthase from *Escherichia coli*. *Struct. Folding Des. 7*, 865–875.
46. Hedstrom, L., and Abeles, R. H. (1988) 3-Deoxy-D-*manno*-octulosonate-8-phosphate synthase catalyzes the C-O bond-cleavage of phosphoenolpyruvate. *Biochem. Biophys. Res. Commun. 157*, 816–820.
47. DeLeo, A. B., Dayan, J., and Sprinson, D. B. (1973) Purification and kinetics of tyrosine-sensitive 3-deoxy-D-*arabino*-heptulosonic acid 7-phosphate synthetase from *Salmonella*. *J. Biol. Chem. 248*, 2344–2353.
48. Shulami, S., Furdui, C., Adir, N., Shoham, Y., Anderson, K. S., and Baasov, T. (2004) A reciprocal single mutation affects the metal requirement of 3-deoxy-D-*manno*-2-octulosonate-8-phosphate (KDO8P) synthases from *Aquifex pyrophilus* and *Escherichia coli*. *J. Biol. Chem. 279*, 45110–45120.
49. Kumar Sau, A., Li, Z., and Anderson, K. S. (2004) Probing the role of metal ions in the catalysis of *Helicobacter pylori* 3-deoxy-D-*manno*-octulosonate-8-phosphate synthase using transient kinetic analysis. *J. Biol. Chem. 279*, 15787–15794.
50. Duewel, H. S., and Woodard, R. W. (2000) A metal bridge between two enzyme families. 3-Deoxy-D-*manno*-octulosonate-8-phosphate synthase from *Aquifex aeolicus* requires a divalent metal for activity. *J. Biol. Chem. 275*, 22824–22831.
51. Walker, S. R., and Parker, E. J. (2006) Synthesis and evaluation of a mechanism-based inhibitor of a 3-deoxy-D-*arabino* heptulosonate 7-phosphate synthase. *Bioorg. Med. Chem. Lett. 16*, 2951–2954.
52. Kaustov, L., Kababya, S., Belakhov, V., Baasov, T., Shoham, Y., and Schmidt, A. (2003) Inhibition mode of a bisubstrate inhibitor of KDO8P synthase: a frequency-selective REDOR solid-state and solution NMR characterization. *J. Am. Chem. Soc. 125*, 4662–4669.
53. Wang, J., Duewel, H. S., Woodard, R. W., and Gatti, D. L. (2001) Structures of *Aquifex aeolicus* KDO8P synthase in complex with R5P and PEP, and a bisubstrate inhibitor: role of active site water in catalysis. *Biochemistry 40*, 15676–15683.
54. Asojo, O., Friedman, J., Adir, N., Belakhov, V., Shoham, Y., and Baasov, T. (2001) Crystal structures of KDO8P synthase in its binary complexes with the substate phosphoenolpyruvate and with a mechanism-based inhibitor. *Biochemistry 40*, 6326–6334.
55. Grison, C., Petek, S., Finance, C., and Coutrot, P. (2005) Synthesis and antibacterial activity of mechanism-based inhibitors of KDO8P synthase and DAH7P synthase. *Carbohydr. Res. 340*, 529–537.
56. Priestman, M. A., Healy, M. L., Becker, A., Alberg, D. G., Bartlett, P. A., Lushington, G. H., and Schönbrunn, E. (2005) Interaction of phosphonate analogues of the tetrahedral reaction intermediate with 5-enolpyruvylshikimate-3-phosphate synthase in atomic detail. *Biochemistry 44*, 3241–3248.